TechMecha RoboSphere | 2026, Vol. 1, No.1, 75 – 88 | ISSN Online: 3155-6019
DOI: https://doi.org/10.62718/vmca.tech-robo.1.1.SC-0126-002

VMC ANALYTIKS

OPEN ACCESS

Minimalistic LoRaWAN Communication: Solar Cell Configuration with Lithium Battery Characterization at Low Solar Irradiance

Article History:

Initial submission:	19 March 2026
First decision:	30 March 2026
Revision received:	22 July 2026
Accepted for publication:	30 July 2026
Online release:	07 August 2026

Jeffrey O. Aquino[1]
Wilfredo D. Timajo[1], DEng

[1]Faculty, College of Engineering, Rizal Technological University, Boni Avenue, Mandaluyong City, Philippines

Abstract

Solar-powered electronics equipment/gadgets have been available for mobile as well as stationary applications. Yet, there are a multitude of unrealistic, advertised duration of usage for a specific load requirement that necessitated the inclusion of a back-up battery to sustain continuous load supply, specifically at diminished solar irradiance. The present study made use of experimental research design where relationships in rate of rise in charging voltage, energy discharge for lithium battery variants and 0.5V solar cells were observed at the highest and lowest solar irradiance with and without boost converter. Temperature, as determined to affect semiconductor performance, was maintained at 25 deg.C. The 0.5V cells were connected in series to achieve 4.5 V open-circuit voltage while connecting these modules up to 5 parallel configurations (termed as 1 module) to increase the current density. Using Kruskal Wallis test for significance and Dunn's post-hoc test for pairwise comparison, the results revealed that at 19W/m2 (low solar irradiance), there is a significant difference in voltages, probably, due to the voltage drop inherent to the booster design with inductor. The energy density (Wh/kg) of lithium battery variants e.g. Lithium Manganate etc. were confirmed to agree on the findings stated in the literature and the power density (W/kg) of lithium iron phosphate appear to agree, as well. The microcontroller for LoRa used as test load required 3.3 volts consuming 70 – 110 mA. The 4.5-V module was able to supply 5.5mA at low solar irradiance (19W/m2) hence necessitating, at least, 16 shunt modules to operate without a battery. The test was made using 12 shunt modules and joystick coordinate was transmitted. However, with visible flicker which was partially eliminated thru a shunt filter capacitor. Data reception reached 34m with obstruction while increasing the solar irradiance to 30W/m2 consequently increased the communication distance to better than 164m. The results emphasize that stable power delivery rather than raw current magnitude, is the critical factor in enabling reliable solar-powered LoRa operation under low-irradiance conditions. Further test is recommended to determine the maximum transmission and reception distance using 16 modules or more to guarantee remote sensing data integrity and latency at the lowest solar irradiance of 19W/m2.

Keywords: Solar Cell Boost Converter, Solar-powered LoRa, Lithium Batteries for LoRa

INTRODUCTION

Solar energy has emerged as a critical power source for remote Internet of Things (IoT) applications, particularly in off-grid environments where traditional electrical infrastructure is unavailable or impractical. The proliferation of low-power wide-area network (LPWAN) technologies, especially LoRa (Long Range) has enabled wireless communication over extended distances with minimal energy consumption, making it an ideal candidate for solar-powered remote sensing, agricultural monitoring, smart infrastructure, and environmental data collection. However, the practical deployment of solar-powered LoRa nodes faces significant challenges under low solar irradiance conditions, which are common during overcast weather, early mornings, late afternoons, and in regions with limited sunlight exposure.

While extensive research has focused on solar cell efficiency under standard test conditions (STC) of 1000 W/m², comparatively few studies have systematically characterized the performance of low-cost photovoltaic systems under weak illumination conditions. This gap is particularly relevant for minimalist IoT node designs, where commercial solar panels often fail to meet their advertised specifications when operating at diminished irradiance levels. The discrepancy between nameplate ratings and actual field performance frequently necessitates the inclusion of backup batteries to sustain continuous load supply, yet the specific configurations required for reliable operation remain insufficiently quantified.

Furthermore, existing literature has explored individual aspects of solar-powered systems, including battery chemistry selection (Khairunnisa et al., 2021), boost converter efficiency (Babaa et al., 2018), and LoRaWAN adaptive data rate optimization (Kufakunesu et al., 2020). However, few studies have integrated these components into a unified experimental framework that examines the interactions between solar cell configuration, power conversion losses, battery discharge characteristics, and communication reliability under realistic low-irradiance conditions. The relationship between available harvested power and LoRa transmission range, particularly under energy-constrained scenarios, remains poorly understood.

This study addresses this gap by measuring the performance of series-parallel-connected 0.5 V solar cells in two critical applications: (1) charging lithium-based batteries under low irradiance, and (2) directly powering an ESP32 LoRa module without battery backup. Specifically, this research aims to:

1. Determine the charging characteristics of four lithium battery chemistries (NMC, NCA, IMR, and IFR/$LiFePO_4$) when powered by a solar module configuration under low irradiance (19 W/m²), with and without a Joule Thief boost converter.

2. Evaluate the energy discharge performance of different lithium battery variants under load conditions approximating LoRa microcontroller operation.

3. Quantify the maximum transmission and reception distance achievable by a solar-powered ESP32 LoRa node under low irradiance conditions and assess the relationship between solar module count and communication reliability.

4. Compare the effect of increased solar irradiance (from 19 W/m² to 30 W/m²) on communication range and system stability.

By determining the optimal solar cell configuration for these tasks, this work provides a practical framework for designing energy-efficient, off-grid LoRaWAN systems in low-sunlight environments. The findings will aid in calculating the required solar panel sizing and battery support for reliable operation, benefiting remote sensing applications, precision agriculture, environmental monitoring, and smart infrastructure deployments in regions with variable solar insolation. The results are expected to guide both system designers in selecting appropriate battery chemistries and developers in sizing photovoltaic arrays to ensure data integrity and acceptable communication range under the most challenging lighting conditions.

LITERATURE REVIEW

To situate "Minimalistic LoRaWAN Communication: Solar Cell Configuration with Lithium Battery Characterization at Low Solar Irradiance," it is essential to frame how low-irradiance energy harvesting limits both power delivery and communication reliability in solar-powered IoT systems. In off-grid LoRa deployments, the primary constraint is not only average harvested energy but also the system's ability to sustain instantaneous current demand during transmission events. Because low-cost, small-area solar cells are commonly used in minimalist sensor nodes, understanding how irradiance, series–parallel cell configuration, converter losses, and battery chemistry interact becomes crucial in determining whether a LoRa microcontroller can operate battery-assisted or stand-alone, and what solar sizing is required to preserve data integrity and acceptable range. Against this backdrop, the following review synthesizes prior work on solar cell behavior under weak illumination, current gains from parallel configurations, converter performance limits, battery discharge behavior under load, and LoRa link adaptation mechanisms that directly inform the study's configuration choices and interpretation.

Context: Low-Irradiance Solar Output and Semiconductor Limits. To begin with, solar cells operate as semiconductor devices whose voltage and current outputs degrade as illumination decreases. Under weak light, internal and recombination-related losses become more influential, reducing both usable voltage and harvestable current. Prior experimental work shows that reduced light intensity decreases open-circuit voltage (Voc) and short-circuit current (Isc), consistent with the idea that effective internal resistance increases as irradiance drops (Olson, 2023). Related analyses further attribute Voc reduction at low light to changes in recombination resistance that dominate device behavior under weak illumination, diminishing power output even when temperature is held constant (Pepa, 2025). This foundational behavior explains why low solar irradiance can prevent small panels from directly sustaining microcontrollers and radio loads without careful configuration.

Parallel Module Configuration as a Practical Current-Density Strategy. Moreover, one commonly applied design response to low-light limitations is increasing current density through parallel connections. While simple linear scaling is often assumed (i.e., identical strings in parallel yield proportional current), empirical measurements frequently show deviations due to reductions in effective resistance and improved charge transport when modules share the load. Studies on series–parallel photovoltaic configurations report measurable changes in output characteristics when strings are combined, supporting the design rationale that parallelization can reduce losses and improve delivered current beyond naive linear expectations (Yusof & Baharuddin, 2020). Reviews emphasizing thermal and resistive effects likewise support the idea that configuration-dependent losses materially influence PV output, especially when operating far from peak irradiance conditions (Shaker et al., 2024). In minimalist LoRa nodes, this makes parallel "module stacking" a direct pathway to meeting radio current requirements without increasing cell voltage beyond safe charging limits.

Boost Converter Limitations Under Weak Harvesting Conditions. Although boost converters are often introduced to maintain usable voltage, converter effectiveness depends on sufficient input power. Under low irradiance, the converter may behave less like an ideal step-up device and more like an added impedance that reduces delivered voltage and usable energy. Overviews of boost converters in PV contexts highlight that efficiency and achievable regulation are highly sensitive to input conditions, particularly when the PV source cannot provide adequate current to support switching demands (Babaa et al., 2018). Related renewable-energy converter design work also notes that low input voltage and poor illumination can increase stress and reduce stability of the delivered output, limiting the converter's ability to preserve consistent voltage at the load (Salim et al., 2022). In a LoRa power chain, these constraints matter because transmission events create short-duration current spikes; if the converter cannot maintain output under those conditions, the system experiences brownouts, resets, or unstable transmission.

Battery Performance Under Low-Irradiance Charging and High-Pulse Loads. Consequently, battery chemistry becomes central in low-irradiance solar systems because the battery must buffer energy between harvest periods and transmission bursts. Comparative discharge studies show that chemistries differ substantially in voltage stability and energy delivery under load, which affects whether a node can maintain radio operation as voltage drops. Work on using batteries in small generating systems demonstrates that discharge behavior and delivered energy can vary markedly among lithium chemistries and use cases (Khairunnisa et al., 2021). Industry-facing comparisons further emphasize that $LiFePO_4$ (LFP) tends to maintain steadier voltage under load than many Li-ion variants, improving usability in power-buffered solar systems where stable regulation matters (Ufine Battery, 2024; Vatrer Power, 2024). From a system-design perspective, this supports evaluating not just nominal capacity but *usable discharge duration at the radio's operating current*, which is the practical determinant of remote-node uptime.

Battery Chemistry Tradeoffs for Burst vs. Sustained Power Delivery. Results also align with the broader engineering distinction between chemistries optimized for energy density versus power delivery and stability. Modeling work on lithium batteries and their behavior during parallel charging underscores that electrical behavior under load and charging regimes is not uniform across chemistries, and that system design must reflect those differences (Shieh et al., 2022). Complementary technical summaries describe how certain chemistries can tolerate higher burst currents but may exhibit faster voltage sag under sustained load, which becomes critical when powering radios that operate near minimum voltage thresholds. These tradeoffs are directly relevant when deciding whether a LoRa node should be designed around sustained daytime operation (solar-direct) or continuous 24-hour operation (solar + battery buffering).

LoRaWAN Link Reliability Under Energy Constraints. Finally, the communication layer is not independent of the power layer: LoRaWAN performance and achievable range depend on both radio parameters and available energy during transmissions. Surveys of LoRaWAN Adaptive Data Rate (ADR) show that link settings can be adjusted to balance range, airtime, and reliability, which in turn changes energy consumption per message (Kufakunesu et al., 2020). Practical LoRaWAN overviews likewise describe how link-budget adjustments and configuration choices influence successful communication distance under varying conditions (Delighteck, 2025). In minimalist solar-powered nodes, this means that improved harvested current (via configuration or irradiance increase) can translate into greater operational stability and range, not simply because "more power is available," but because the system can sustain more robust transmission settings without voltage collapse.

Taken together, these strands of literature motivate the study's focus on series–parallel solar cell configuration, converter inclusion/exclusion under weak light, battery chemistry comparison under realistic radio-equivalent loads, and range testing under low irradiance all aimed at establishing practical design rules for LoRa nodes that must operate reliably in low-sunlight environments.

METHODS

This study employed an experimental research design to evaluate the performance of low-cost, micro-scale solar cells for (1) charging lithium-based batteries and (2) directly powering a LoRa-enabled microcontroller under low solar irradiance. The photovoltaic (PV) system consisted of 0.5 V monocrystalline solar cells configured in series and parallel combinations. Each string comprised nine (9) series-connected cells (nominal open-circuit voltage of 4.5 V), and one module consisted of five (5) parallel-connected strings. Multiple modules (1, 3, and 12 modules) were connected in parallel to increase available current. Tests were conducted with and without a Joule Thief boost converter to assess the impact of conversion losses on charging and load stability.

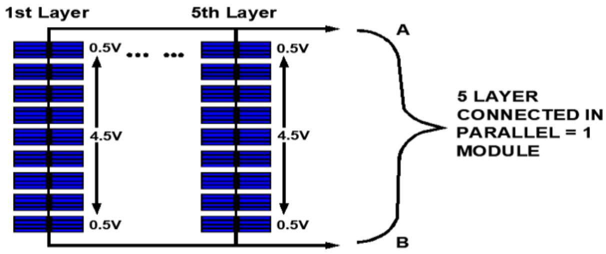

Figure 1
One (1) module = shunt connection of five (5) 4.5V layers

Four lithium battery chemistries were evaluated: lithium nickel manganese cobalt oxide ($LiNiMnCoO_2$, NMC), lithium nickel cobalt aluminum oxide ($LiNiCoAlO_2$, NCA), lithium manganese oxide ($LiMn_2O_4$, IMR), and lithium iron phosphate ($LiFePO_4$, IFR). For load testing, an LED module and an ESP32 LoRa microcontroller were used to approximate the operating current of a typical LoRa node (70–110 mA at 3.3 V).

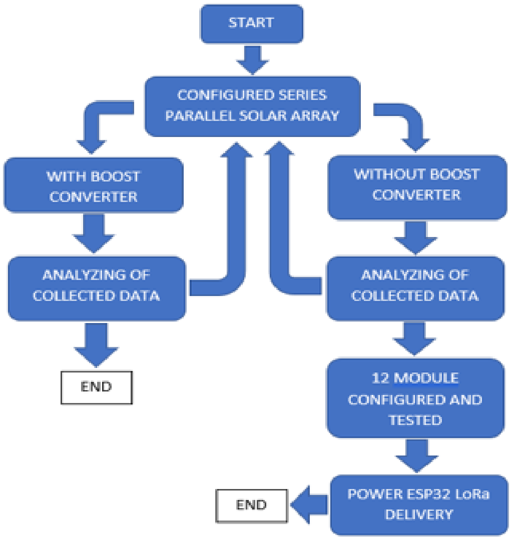

Figure 2
Experimental Flowchart for Photovoltaic Configuration and Load Testing

The flowchart summarizes the procedural sequence including series–parallel configuration of 0.5 V solar cells, boost converter inclusion or exclusion, voltage and current measurement, battery charging evaluation, and direct ESP32 LoRa powering tests under controlled irradiance.

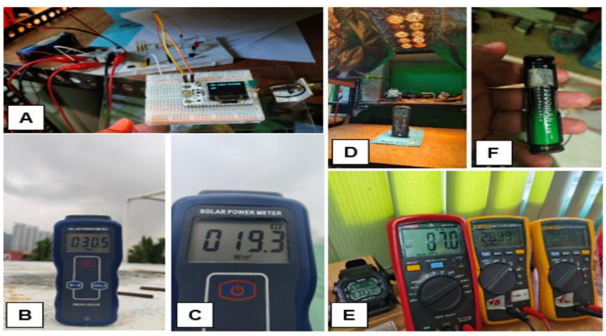

Figure 3
Experimental Instrumentation and Validation Setup under Low Irradiance

(A) ESP32 LoRa microcontroller used as active load, (B) solar irradiance meter for outdoor validation, (C) reference low-irradiance measurement (~19 W/m²), (D) controlled indoor irradiance simulation chamber, (E) digital multimeters for voltage and current monitoring, and (F) lithium battery chemistry evaluated for charging and discharge characterization.

Irradiance Measurement and Test Conditions. Solar input was quantified using irradiance (W/m²) rather than illuminance-related measures. Irradiance was recorded continuously over a seven-day period from sunrise to sunset using a calibrated solar irradiance meter. Based on these measurements, 19 W/m² was identified as the representative low-irradiance condition for laboratory and field testing, while higher irradiance conditions (up to 30 W/m²) were used for comparative range measurements. During each test condition, irradiance was logged at 1-minute intervals to capture short-term variability.

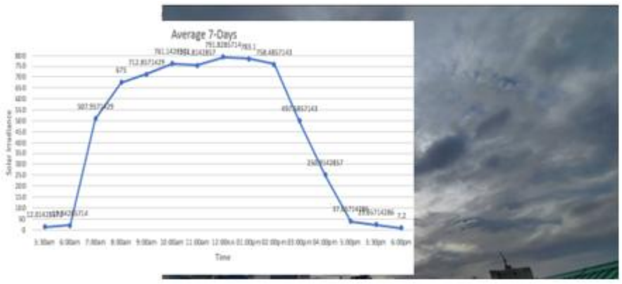

Figure 4
Low and High Solar Irradiance Data for 7 days observation

Sample Sizes, Measurement Intervals, and Data Collection. Each electrical configuration (1, 3, and 12 modules; with and without boost converter) was tested in five (n = 5) repeated trials. Voltage and current measurements were recorded at 1-minute intervals during charging and discharge experiments. For battery discharge tests, measurements continued until the terminal voltage dropped to 2.8 V. For LoRa transmission tests, packet transmission success was recorded over fixed-distance intervals (5 m increments) under both line-of-sight and obstructed conditions. Reported values represent mean measurements across trials, with observed variability within ±5–10% across repeated runs.

Finally, the shunted battery was removed, and the cells were connected directly to the LoRa microcontroller as actual load, tested by sending analog joystick data. Accurate data transmission and reception served as the base criterion in qualifying the effective distance under line-of-sight (LOS) and obstructed conditions at 19 W/m2.

Data collection included measurement of voltage, current, irradiance, and packet delivery metrics. Statis- tical analysis used the Kruskal-Wallis H test to identify performance differences across battery types, with Dunn's post-hoc test for pairwise comparisons. Latency in data transmission was not considered in the present study.

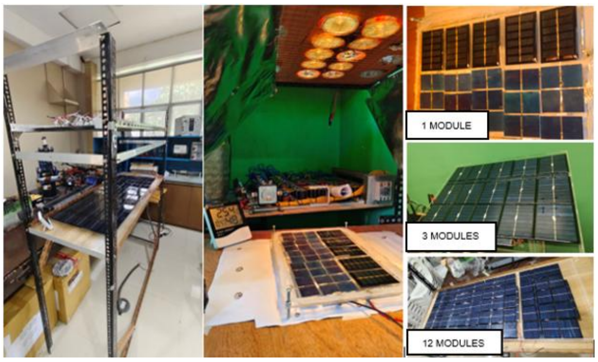

Figure 5
Photovoltaic Module Configurations used in Low-irradiance Testing

At ~19 W/m², we tested two PV arrays: 12 parallel modules (9×0.5 V series=4.5 V/module) and one module (5 × (9×0.5 V series) in-parallel). We measured Voc and loaded V/I on ESP32-LoRa (3.3 V, 70–110 mA) with/without Li batteries; n=5/configured; ~25 °C; panel-surface-temp monitored; no thermal control; Kruskal–Wallis, Dunn's post-hoc.

Temperature Monitoring and Control. Ambient laboratory temperature was maintained at approximately 25 °C throughout the experiments see Fig. 5. The operating temperature of the solar cells was monitored using a digital surface thermometer placed near the cell surface to distinguish between ambient temperature and panel temperature. No active thermal regulation of the solar cells was implemented; therefore, reported temperature conditions refer to ambient laboratory temperature rather than exact photovoltaic junction temperature. This distinction is important, as PV performance is influenced by device temperature rather than ambient air temperature alone.

Schematic Diagram

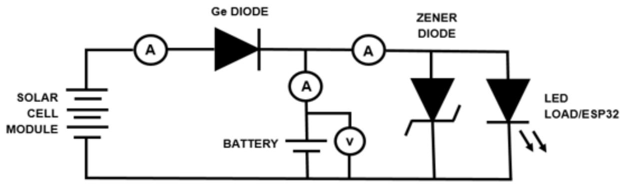

Figure 6
Circuit Diagram for Solar Charger System Without Booster Converter

The schematic diagram illustrates a solar charging circuit without a boost converter designed to power a load such as an ESP32 LoRa module or LED while charging a lithium battery. The system operates directly from the photovoltaic (PV) solar cell module.

The solar cell module serves as the primary energy source generating DC voltage under irradiance. An ammeter is placed in series to measure the current supplied by the solar panel. The output then passes through a germanium (Ge) diode which functions as a blocking diode. This diode prevents reverse current flow from the battery back into the solar panel during low-irradiance or nighttime conditions. A germanium diode is selected due to its lower forward voltage drop compared to standard silicon diodes. Hence, reducing power losses in low-voltage system

RESULTS

Based on the specification of the batteries used, lithium-ion variants are tolerant up to 4.6 V while lithium iron phosphate's cut-off voltage is 3.65 V. An LED module with current consumption equivalent to the ESP32 LoRa transceiver specification (i.e., 3.3 V at 70 mA to 120 mA) was connected as load.

The actual voltage output of the solar module measured at 3.2 V to 3.5 V under loaded condition. Hence, it was determined that the 9 series-connected 0.5 V cells (4.5 V system) may charge lithium battery- ies without overcharging at the highest measured so- lar irradiance of 780 W/m2. The study evaluated the performance of 5 shunt-configured 4.5 V solar mod- ules (1 module = 5 parallel strings, 1 string = 9 series-connected 0.5 V solar cells) under low irradiance (19 W/m2) to charge different battery variants with and without joule thief boost converter.

Table 1

Mean charging rate (Volt/hr) taken using 1 mod- ule (one (1) module = 5 parallel strings, one (1) string = 9 series-connected 0.5V solar cells), generating 5.5mA at 3.3V across each battery type.

Battery Type	Mean Charging Rate (V/hr)	
	Without Boost Converter	With Boost Converter
IFR	0.0362	0.0086
NMC	0.0520	0.0171
NCA	0.0428	0.0332
IMR	0.1746	0.0305

The test is intended to determine if there is significant difference in charging voltages. Test for independent samples indicate that at $p < 0.05$ the charging rate with the boost converter for the 1500 mA · h & 2000 mA · h lithium-iron-phosphate, 3000 mA · h to 10 000 mA · h lithium nickel cobalt/manganese cobalt variants including 8800 mAh AAA alkaline batterie significantly differs from the rate without the boost con- verter, with the latter exhibiting steeper charging slope (V/t).

Table 2

Summary of Energy Discharge by Battery Type at Low Irradiance (19 W/m2) across Load (LED Module)

Battery Type	L1	L2	L3	L4	L5
IFR (Lithium Iron Phosphate Rechargeable)	0.463	1.529	4.263	7.284	8.568
NMC (Lithium Nickel Manganese Cobalt Oxide)	-0.015	0.015	-0.059	-0.001	-0.007
NCA (Lithium Nickel Cobalt Aluminum Oxide)	0.012	8.472	0.012	0.005	0.001
IMR (Lithium-Ion Manganese Rechargeable)	-0.029	-0.031	0.011	-0.001	0.018

The 2600 mAh lithium-ion manganese and 9800 mAh AA alkaline batteries exhibited no notable variation in charging rate with or without a booster. The results imply that the boost converter functioned primarily as complex impedance with the tendency of decreasing the charging voltage available to the batteries.

Kruskal-Wallis H test indicated that there is a significant difference in the discharge energy among battery chemistries at low solar irradiance, $\chi2(4) = 17.16$, $p = .002$, with a mean rank score of 22 for Lithium Iron Phosphate, 5.9 for Lithium Nickel, 12.6 for Lithium Cobalt, 7.1 for Lithium Manganese, and 17.4 for Alkaline.

Post-hoc Dunn's test using a Bonferroni corrected α of 0.005 indicated that the mean ranks of the following pairs are significantly different: lithium iron phosphate and Lithium Nickel (x1 — x2) / lithium iron phosphate and Lithium Manganese (x1 — x4).

Comparison of discharge rates between Lithium-Ion Manganese Rechargeable (IMR, LiMn2O4) and Lithium Iron Phosphate Rechargeable (IFR, LiFePO4) batteries at 19 W/m2 irradiance. The plot shows voltage versus time for both battery chemistries under identical conditions.

Figure 7

Lithium Iron Phosphate battery discharge characteristic when exposed to low solar irradiance supplied using 5 shunted solar modules discharged down to 2.8V beyond 123 mins.

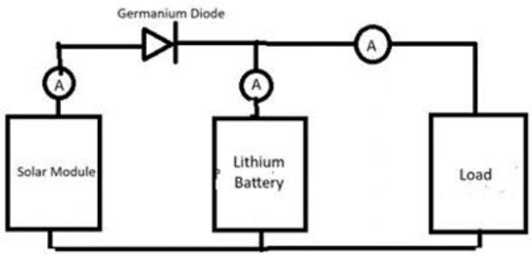

Figure 8

Test jig to measure current generated by single module (1solar module = 5 parallel-connected strings, one string = 9-series-connected 0.5V solar cells), Lithium battery and load without boost converter.

As demonstrated in the sample V-I discharge characteristic, the voltage for the Lithium-Ion Manganese Rechargeable (IMR, $LiMn_2O_4$ MADMASTER) battery decreased in 14 min down to 2.8 V, while Lithium Iron Phosphate Rechargeable (IFR, $LiFePO_4$ BLUE) supplying the same load discharged beyond 123 min.

The test set-up measured the individual current delivered to the load by 3 solar modules and 2 lithium battery variants to approximate the effect of battery chemistry to the discharge duration. The summary is as follows:

Table 3

Summary of current delivered by IMR Battery and 3 solar cell modules at Low Irradiance (19 W/m2) across Load (LED Module)

Lithium Iron Phosphate *Blue* Battery Voltage		Portion of Current (mA) Supplied to the load		Total current to the Load	TIME (min)
Reference	Actual	Solar Cell	Battery		
3.2	3.071	21.8	81.3	103.1	0
3	3	23.2	79.4	102.6	34.43
2.9	2.9	24.2	65.9	90.1	56.17
2.8	2.8	22.77	59.4	82.2	74.46
Mean		**23**			
Lithium Manganese *Madmaster* Battery Voltage		Portion of Current (mA) Supplied to the load		Total current to the Load	TIME (min)
Reference	Actual	Solar Cell	Battery		
3.2	3.139	22.9	57.7	80.6	0
3	3	23.2	57.9	80.1	26.4
2.9	2.9	24.11	33.49	57.6	39.21
2.8	2.8	23.27	29.37	52.4	49.19
Mean		**23.12**			

The current mean for one (1) module is 5.5mA and 22mA for three (3) modules as shown above. The current for the 3 modules, if linearity is assumed, is 5.5mA x 3 = 16.5mA, which connotes that parallel solar cell resistance decreases resulting in increase in delivered current. The Solar Modules with installed Lithium-Ion Battery delivered a sum of 103.1 – 82.2 mA to the load being discharged from 3.071V down to 2.8V in 74.46 mins. while Lithium Manganate battery dispensed 80.6 – 52.4mA at 3.139V down to 2.8V in 49.19 mins. Theoretically, 10 parallel combinations of Lithium-Ion batteries may sustain continuous load operating at 70 – 100mA for 12 hours while the latter may require 15 parallel-connected batteries.

The final test set-up, with the LED load replaced by an ESP32 Lora, was set-up to transmit 12-bit joy- stick coordinates using 5.5mA per module as reference. (1 module=5 shunt-connected strings, each string=9 series-connected 0.5V cell). The study made use of 12 modules and was exposed to 19W/m2 to deliver at least 66mA to an ESP32 LoRa acting as actual load, without using battery back-up. The results indicate functionality over a short distance as indicated below:

Table 4

Ground level signal transmission/reception with obstruction

DISTANCE		STATUS	REMARK
Meter	Elevation		
8.204	Ground Level	Received	confined space
18.01	Ground Level	Received	w/ obstruction
29.95	Ground Level	Received	w/ obstruction
32.64	Ground Level	Received	w/ obstruction
37.07	Ground Level	Received	w/ obstruction
39.03	Ground Level	Received	w/ obstruction, w/ erratic error

The distance covered 37 m maximum at ground level using a 31mm rubber ducky antenna, with obstruction. Results reveal that, at 19 W/m2, accurate data transmission/reception distance was limited at 66 mA, whence increasing to 16 modules will roughly supply 88 mA with an expected proportional increase in communication distance.

Table 5

Ground level signal transmission/reception with obstruction

Mean Distance Elevation		Data Status	Remark
Meter	**Degrees**		
8.204	LOS	Received	within laboratory
25.41	28 Deg.	Received	open space
28.38	25 Deg.	Received	open space
32.92	22 Deg.	Received	open space
41.94	17 Deg.	Received	open space
68.65	10 Deg.	Received	open space
78.31	6 Deg.	Received	open space
85.52	5 Deg.	Received	open space
136.9	< 5 Deg.	Received	with obstruction
164.1	< 5 Deg.	Received	with obstruction

Further increase in solar irradiance to 30 W/m2 resulted in an increase better than 164 m transmission/reception distance at various subtended angles of elevation, with- out and with obstruction. It may be noted that the increase in solar irradiance from 19 W/m2 to 30 W/m2 increased the distance from 37 m to better than 164 m.

DISCUSSION

Solar Cell Performance Under Low Illumination. The experimental findings confirm the fundamental behavior of photovoltaic devices under diminished lighting conditions, consistent with established semiconductor theory. When solar irradiance decreases, the internal resistance of the solar cell increases, which reduces the usable energy reaching the load and lowers the output voltage. This behavior aligns with the work of Olson (2023), who experimentally demonstrated that reduced light intensity decreases both open-circuit voltage (Voc) and short-circuit current (Isc) due to increased internal resistance effects. Similarly, Pepa (2025) attributed Voc reduction under weak illumination to heightened recombination resistance (Rrec), which dominates device behavior and degrades power output even when temperature is held constant. These theoretical considerations provide the foundation for interpreting the observed performance of the 0.5 V solar cells under the low-irradiance condition of 19 W/m² employed in this study.

Parallel Module Configuration. The current output enhancement observed from parallel module configurations supports the non-linear scaling behavior reported in previous photovoltaic studies. As presented in the Results section, the mean current output for a single module was 5.5 mA, while three parallel-connected modules yielded 22.81 mA. Under linear scaling assumptions (5.5 mA × 3 = 16.5 mA), the observed 38% increase indicates a significant non-linear enhancement in current output. This deviation can be attributed to reduced internal resistance in parallel configurations, which improves charge carrier mobility and lowers energy losses, a phenomenon documented by Yusof and Baharuddin (2020) and further supported by Shaker et al. (2024) in their comprehensive review of thermal and resistive effects on PV output. The practical implication for minimalist LoRa node design is that parallel "module stacking" provides a direct pathway to meeting radio current requirements without exceeding safe charging voltage limits.

Boost Converter Limitations. The experimental results indicate that the Joule Thief boost converter functioned primarily as an added impedance rather than an effective voltage step-up device under low-irradiance conditions. As shown in Table 1, charging rates across all battery types were consistently lower when the boost converter was included compared to direct charging configurations. For instance, the IFR battery exhibited a charging rate of 0.0362 V/hr without the converter versus 0.0086 V/hr with the converter, representing a 76% reduction in charging efficiency.

These findings are consistent with the limitations of boost converters under weak harvesting conditions documented in the literature. Babaa et al. (2018) highlighted that conventional boost converters exhibit reduced efficiency under low irradiance, as their voltage step-up capability is constrained by diminished input current. The low solar irradiance reduces the effective voltage input to the converter, limiting its ability to compensate for voltage drops during battery charging cycles (Colucci & Mahgoub, 2025). Furthermore, Salim et al. (2022) noted that low input voltage from solar panels under poor illumination increases switch stress in boost converters, reducing their ability to maintain consistent output voltage and mitigate charging anomalies such as the rubber band effect. In the present study, the boost converter's inability to improve charging performance under 19 W/m² irradiance suggests that direct solar-to-battery connection is more effective for low-light applications, despite the potential for overcharging at higher irradiance levels.

Battery Performance Comparison. The Kruskal-Wallis test results, as presented in the Results section, revealed significant differences in discharge energy among battery chemistries at low solar irradiance, $\chi^2(4) = 17.16$, $p = .002$, with mean rank scores of 22 for Lithium Iron

Phosphate (IFR), 5.9 for Lithium Nickel (NMC), 12.6 for Lithium Cobalt (NCA), 7.1 for Lithium Manganese (IMR), and 17.4 for Alkaline. Post-hoc Dunn's test using a Bonferroni-corrected α of 0.005 further identified significant differences between IFR and NMC ($x_1 - x_2$) and between IFR and IMR ($x_1 - x_4$).

These findings align with the comparative discharge study by Khairunnisa et al. (2021), whose tests showed that $LiFePO_4$ batteries delivered substantially higher usable energy compared to standard Li-ion variants. The superior performance of IFR batteries under load conditions is corroborated by industry comparisons from Ufine Battery (2024) and Vatrer Power (2024), which demonstrate that LFP batteries maintain steadier voltage under load than many Li-ion alternatives, making them particularly suitable for power-buffered solar systems where stable regulation is critical. From a system-design perspective, these results support evaluating not just nominal capacity but usable discharge duration at the radio's operating current, the practical determinant of remote-node uptime.

Battery Chemistry Tradeoffs for Burst vs. Sustained Power Delivery. The discharge characteristics observed between the Lithium-Ion Manganese (IMR) and Lithium Iron Phosphate (IFR) batteries further illustrate the engineering tradeoffs between energy density and power delivery stability. As demonstrated in the discharge tests (Figure 7), the IMR battery voltage decreased to 2.8 V within 14 minutes, while the IFR battery supplied the same load for beyond 123 minutes under identical low-irradiance conditions. In the 3-module configuration test (Table 3), the IFR battery maintained a stable output of 103.1 mA to 82.2 mA from 3.071 V down to 2.8 V over 74.46 minutes, whereas the IMR battery delivered 80.6 mA to 52.4 mA from 3.139 V to 2.8 V but lasted only 49.19 minutes.

These results align with Shieh et al. (2022), who found that while ternary chemistries such as NCM811 offer higher energy density (200 Wh/kg) than $LiFePO_4$, they require stricter thermal controls and exhibit faster voltage sag under sustained load. Battery University's findings further explain that LMO batteries can handle high-current bursts but exhibit faster capacity fade and more rapid voltage drop under load, accounting for the observed steeper current decline in the IMR batteries. For LoRa nodes operating near minimum voltage thresholds, these tradeoffs are critical when deciding between sustained daytime operation (solar-direct) and continuous 24-hour operation (solar + battery buffering).

LoRaWAN Performance Under Energy Constraints. The communication layer performance demonstrated a clear relationship between available harvested power and achievable range. At 19 W/m² solar irradiance with 12 modules delivering 66 mA, the system achieved a maximum transmission and reception distance of 37 m with obstruction. The projected scaling to 16 modules (88 mA) suggests a proportional extension in communication distance, while increasing irradiance to 30 W/m² enhanced the operational range to 164 m—a 340% improvement.

This relationship underscores that improved harvested current translates into greater operational stability and range, not simply because "more power is available," but because the system can sustain more robust transmission settings without voltage collapse. In LoRa systems, achievable communication range is fundamentally governed by radio parameters such as transmit power, spreading factor, bandwidth, coding rate, and receiver sensitivity, which together define the link budget.

These findings align with LoRaWAN's Adaptive Data Rate (ADR) mechanism, which dynamically optimizes spreading factors (SF7–SF12) and transmission power to maximize range under varying energy conditions. As documented by Kufakunesu et al. (2020), link settings can be adjusted to balance range, airtime, and reliability, which in turn changes energy consumption per message. The LoRa Alliance confirms that ADR adjusts link budgets to sustain connectivity even with fluctuating power inputs (Delighteck, 2025), explaining the observed scalability in transmission distance with higher irradiance.

Future Research Directions. The present study focused on evaluating the solar charger configuration for charging various lithium battery variants, with and without the Joule Thief boost converter, at the lowest solar irradiance of 19 W/m². The performance of the same charger configuration, without the converter and batteries, was evaluated using a LoRa-based microcontroller in terms of transmission and reception distances with and without obstruction.

The findings confirmed that LoRa data acquisition, transmission, and reception may operate in a stand-alone manner during daytime operation. The backup battery types and quantities required for nighttime LoRa operation may be computed based on these results.

However, further evaluation using 16 modules at 19 W/m² solar irradiance is recommended, as the current results were obtained using only 12 modules at this irradiance level. Additionally, while 12 modules at 30 W/m² generated the required energy for transceiver operation, the observed maximum distance of 164 m may not represent the farthest achievable range, as the walkie-talkie radio reference range became unintelligible beyond this distance. The transceiver signal latency observed during testing also warrants further investigation in future studies to ensure data integrity and real-time performance for remote sensing applications.

Theoretical Contributions. This study advances the theoretical understanding of low-irradiance photovoltaic systems for IoT applications through three key findings. First, the observed 38% non-linear enhancement in current output from parallel module configurations (5.5 mA per module versus 22.81 mA for three modules) challenges conventional linear scaling assumptions and provides empirical support for the reduced internal resistance framework proposed by Yusof and Baharuddin (2020) under weak illumination conditions. Second, the significant performance disparity between battery chemistries, where IFR batteries sustaining load for 74.46 minutes versus IMR batteries lasting only 49.19 minutes under identical conditions, demonstrates that usable discharge duration at operating current is a more relevant performance metric than nominal energy density for solar-powered IoT applications. Third, the finding that the Joule Thief boost converter reduced charging rates at 19 W/m² (e.g., IFR: 0.0362 V/hr without converter versus 0.0086 V/hr with converter) contributes to the theoretical discourse on power conversion tradeoffs, suggesting that converter losses may exceed harvesting gains at extremely low irradiance levels, supporting the work of Babaa et al. (2018) and Salim et al. (2022).

Practical Applications. The results provide actionable design guidelines for practitioners deploying solar-powered LoRa networks in low-sunlight environments. The established current output of 5.5 mA per module at 19 W/m² enables accurate solar array sizing: with the ESP32 LoRa consuming 70–110 mA, a minimum of 16 parallel modules is required for stand-alone daytime operation. The discharge duration data allows computation of backup battery requirements for nighttime operation (e.g., approximately 10 parallel IFR batteries for 12-hour operation at 100 mA).

Battery selection criteria are clearly delineated: $LiFePO_4$ (IFR) batteries are preferred for sustained data transmission due to superior voltage stability and extended discharge duration, while IMR batteries, despite higher burst current capability, exhibit rapid voltage sag (2.8 V within 14 minutes) making them unsuitable for reliable long-term deployment. The boost converter findings suggest that direct solar-to-battery connection, with appropriate blocking diodes, is the most efficient configuration for low-light conditions, challenging common industry practices and potentially reducing system costs.

Communication range constraints provide practical deployment parameters: at 19 W/m² with 12 modules (66 mA), reliable transmission is limited to 37 m with obstruction, while increasing irradiance to 30 W/m² extends range to 164 m. This enables site-specific network planning by correlating expected solar irradiance patterns with required communication distances.

Societal and Economic Relevance. This research supports cost-effective, sustainable IoT deployments in underserved regions where electrical infrastructure is limited. The design guidelines facilitate environmental monitoring, agricultural sensing, and disaster preparedness systems using low-cost solar cells, reducing grid dependence and operational costs. The preference for $LiFePO_4$ batteries further promotes sustainability through longer service life and reduced hazardous waste. These findings are particularly relevant for developing regions, enabling data collection for food security monitoring, climate change adaptation, and public health surveillance.

Limitations and Future Directions. The controlled laboratory conditions (25°C ambient temperature) may not fully represent field environments; future studies should investigate combined temperature-irradiance effects. The communication tests using 12 modules at 19 W/m² delivered 66 mA sufficient for basic operation but not optimal transmission parameters; further evaluation with 16 modules is needed to determine maximum achievable range. The transceiver signal latency observed warrants investigation for real-time monitoring applications where data timeliness is critical. Additionally, field-based longitudinal studies examining partial shading, panel soiling, and performance degradation over time would enhance practical applicability.

Conclusion. This study highlights that reliable LoRaWAN communication under low solar irradiance is primarily determined by stable power delivery rather than raw current magnitude. Experimental results showed that parallel module stacking effectively increased current density, enabling minimalist solar arrays to sustain microcontroller loads, while boost converters often introduced impedance losses that reduced charging efficiency under weak illumination. Among the tested chemistries, lithium iron phosphate ($LiFePO_4$) batteries consistently provided the most stable voltage discharge, sustaining ESP32 LoRa operation significantly longer than lithium manganese or nickel-based variants, thereby underscoring their suitability for energy-constrained environments. Communication range testing further revealed that modest increases in irradiance, from 19 W/m² to 30 W/m², substantially extended transmission distance, reinforcing the link between harvested energy stability and network reliability. These findings provide actionable guidance for IoT system designers: prioritize solar module parallelization to maximize current density, select $LiFePO_4$ batteries for buffered operation, minimize reliance on boost converters under low irradiance, and explicitly account for irradiance variability in module sizing to preserve data integrity and communication range. By applying these design rules, developers can enhance the resilience of solar-powered LoRaWAN nodes, enabling more reliable remote sensing, agricultural monitoring, and smart infrastructure applications in regions with limited sunlight exposure.

Author contributions. Wilfredo L. Timajo - Conceptualization, Writing-review & editing, Validation, Data curation | Jeffrey O. Aquino - Investigating, Project administration, Writing original draft, Resources.

Conflict of interest. The authors declare that the research was conducted in the absence of any commercial, financial, or personal relationships that could be construed as a potential conflict of interest.

Funding source. No external funding, grants, or institutional support were received that would have influenced the study design, data collection, analysis, or interpretation of results. The authors have no patents, product

development, or consultancy roles related to the materials or technologies discussed in this work. All experimental procedures and findings are reported with full objectivity and transparency. All expenses related to materials, equipment, laboratory access, and consumables were personally borne by the authors.

Artificial intelligence use. The authors used ChatGPT and DeepSeek exclusively for language refinement, grammar correction, and phrase arrangement to improve the clarity and readability of the manuscript. No AI tools were employed for experimental design, data collection, statistical analysis, result interpretation, or drawing scientific conclusions. All experimental data, measurements, and findings reported in this study originate strictly from the authors' actual laboratory work. The authors have critically reviewed and revised all AI-assisted text and assume full responsibility for the accuracy, originality, and scientific integrity of the final manuscript.

Ethics approval statement. This study was approved by the RTU - Research Ethics Committee, with approval number 2024-29.

Data availability statement. The datasets generated and/or analyzed during the current study, including raw voltage, current, irradiance, and communication distance logs, are not publicly deposited in a repository but are available from the corresponding author upon reasonable request, subject to the authors' institutional data retention policies.

Acknowledgement. (Not available)

Publisher's disclaimer. The views expressed in this article are those of the authors and do not necessarily reflect the views of the publisher. The publisher disclaims any responsibility for errors or omissions.

REFERENCES

Babaa, S., Murr, G., Mohamed, F., & Pamuri, S. (2018). Overview of boost converters for photovoltaic systems. *Journal of Power and Energy Engineering, 6*(4), 16–31. https://doi.org/10.4236/jpee.2018.64002

Battery University. (n.d.). *BU-205: Types of lithium-ion*. Cadex Electronics. https://batteryuniversity.com/article/bu-205-types-of-lithium-ion

Colucci, R., & Mahgoub, I. (2025). Generalizable solar irradiance prediction for battery operation optimization in IoT-based microgrid environments. *Journal of Sensor and Actuator Networks, 14*(1), 3. https://doi.org/10.3390/jsan14010003

Delighteck. (2025, March 20). *LoRaWAN technical overview part 3* [Blog post]. Delighteck. https://www.delighteck.com/blogs/lorawan-technical-overview-part3

Khairunnisa, K., Fahmi, H., & Suryanegara, M. (2021). Utilization of used electric vehicle batteries for the design of mini-generating systems. *Journal of Physics: Conference Series, 2111*(1), 012050. https://doi.org/10.1088/1742-6596/2111/1/012050

Kufakunesu, R., Hancke, G. P., & Abu-Mahfouz, A. M. (2020). A survey on adaptive data rate optimization in LoRaWAN. *Sensors, 20*(18), 5044. https://doi.org/10.3390/s20185044

Olson, A., & Finio, B. (2023). *How does solar cell output vary with incident light intensity?* Science Buddies. https://www.sciencebuddies.org/science-fair-projects/project-ideas/EnergyP014/energy-power/how-does-solar-cell-output-vary-with-incident-light-intensity

Pepa, P. E., Afungchuia, D., Holtomoa, O., & Ebobenow, J. (2025). Parameters critically affecting the open circuit voltage of an organic solar cell. *Heliyon, 11*(4), e42684. doi: 10.1016/j.heliyon.2025.e42684

Salim, K., Asif, M., Ali, F., Armghan, A., Ullah, N., Mohammad, A.-S., & Al Ahmadi, A. A. (2022). Low-stress and optimum design of boost converter for renewable energy systems. *Micromachines, 13*(7), 1085. https://doi.org/10.3390/mi13071085

Shaker, L. M., Al-Amiery, A. A., Hanoon, M. M., Al-Azzawi, W. K., Kadhum, A. A. H. (2024). Examining the influence of thermal effects on solar cells: A comprehensive review. *Sustainable Energy Research, 11*(1), 6. https://link.springer.com/article/10.1186/s40807-024-00100-8

Shieh, Y.-T., Wu, C.-C., Liu, C.-Y., Chieng, W.-H., Su, Y.-S., Jeng, S.-L., & Chang, E.-Y. (2022). Lithium battery model and its application to parallel charging. *Energies, 15*(13), 4767. https://doi.org/10.3390/en15134767

Ufine Battery. (2024, January 19). *LiFePO4 battery vs. lithium-ion polymer battery: Key differences explained*. https://www.ufinebattery.com/blog/lifepo4-battery-vs-lithium-ion-polymer-battery/

Vatrer Power. (2024, April 30). *LiFePO4 battery vs. lithium-ion battery: An in-depth comparison*. https://www.vatrerpower.com/en-de/blogs/news/lifepo4-battery-vs-lithium-ion-battery-an-in-depth-comparison

Yusof, N. B. M., & Baharuddin, A. B. (2020). The study of output current in photovoltaics cell in series and parallel connections. *International Journal of Technology, Innovation and Humanities, 1*(1), 7–12.